

Artificial intelligence for rapid identification of the coronavirus disease 2019 (COVID-19)

Xueyan Mei^{1,16}, Hao-Chih Lee^{2,16}, Kaiyue-Diao^{3,16}, Mingqian Huang⁴, Bin Lin⁵, Chenyu Liu¹, Zongyu Xie⁶, Yixuan Ma¹, Philip M. Robson^{1,4}, Michael Chung⁴, Adam Bernheim⁴, Venkatesh Mani^{1,4}, Claudia Calcagno^{1,4}, Kunwei Li⁷, Shaolin Li⁷, Hong Shan⁷, Jian Lv⁸, Tongtong Zhao⁹, Junli Xia¹⁰, Qihua Long¹¹, Sharon Steinberger⁴, Adam Jacobi⁴, Timothy Deyer^{12,13}, Marta Luksza¹⁴, Fang Liu¹⁵, Brent P. Little^{15,17*}, Zahi A. Fayad^{1,4,17*}, Yang Yang^{1,4,17*}

¹BioMedical Engineering and Imaging Institute, Icahn School of Medicine at Mount Sinai, New York, NY, USA

²Department of Genetics and Genomic Sciences, Icahn School of Medicine at Mount Sinai, New York, NY, USA

³Department of Radiology, West China Hospital, Sichuan University, Chengdu, Sichuan, China

⁴Department of Diagnostic, Molecular and Interventional Radiology, Icahn School of Medicine at Mount Sinai, New York, NY, USA

⁵Department of Radiology, The Second Affiliated Hospital of Zhejiang University, Hangzhou, Zhejiang Province, China

⁶Department of Radiology, The First Affiliated Hospital of Bengbu Medical College, Bengbu, Anhui, China

⁷Guangdong Provincial Key Laboratory of Biomedical Imaging, The Fifth Affiliated Hospital of Sun Yet-sen University, Zhuhai, Guangdong, China

⁸Department of Radiology, Nanxishan Hospital, Guangxi Zhuang Autonomous Region, China

⁹Department of Radiology, The Second People's Hospital, Fuyang, Anhui, China

¹⁰Department of Radiology, Bozhou Bone Trauma Hospital Image Center, Bozhou, Anhui, China

¹¹Department of Radiology, Remin Hospital of Wuhan University, Wuhan, Hubei, China

¹²East River Medical Imaging, New York, NY, USA

¹³Department of Radiology, Weill Cornell Medicine, New York, NY, USA

¹⁴Department of Oncological Sciences, Icahn School of Medicine at Mount Sinai, New York, New York, USA

¹⁵Department of Radiology, Massachusetts General Hospital, Boston, MA, USA

¹⁶These authors contributed equally: Xueyan Mei, Hao-Chil Lee, Kaiyue Diao.

¹⁷ Corresponding authors. These authors jointly supervised this work: Brent P. Little, Zahi A.

Fayad, Yang Yang. *email: blittle@partners.org, zahi.fayad@mssm.edu, yang.yang@mssm.edu.

Abstract

The coronavirus disease 2019 (COVID-19) outbreak that originated in Wuhan, China has rapidly propagated due to widespread person-to-person transmission and has resulted in over 1,133,758 cases in 197 countries with a total of 62,784 deaths as of April 5, 2020. Laboratory confirmation of SARS-CoV-2 is performed with a virus-specific reverse transcriptase polymerase chain reaction (RT-PCR) test. This test can take up to two days to complete, and, due to the possibility of false negatives, serial testing may be required to reliably exclude infection. A current supply shortage of RT-PCR test kits compounds the shortcomings of entrusting diagnosis to the PCR test alone and underscores the urgent need to provide alternative methods for the rapid and accurate diagnosis of SARS-CoV-2 patients. Chest computed tomography (CT) is a valuable component in the evaluation of patients with suspected SARS-CoV-2 infection. Nevertheless, CT alone may have limited negative predictive value to fully exclude infection, because of the normal radiologic findings in some early disease patients. In this study, we use artificial intelligence (AI) algorithms to integrate chest CT findings with clinical symptoms, exposure history, and/or laboratory testing to more accurately and rapidly diagnose SARS-CoV-2 (+) patients. We included 905 RT-PCR confirmed patients. 419 (46.2%) tested positive for SARS-CoV-2 by laboratory-confirmed real-time RT-PCR assay and next-generation sequencing, while 486 patients (53.8%) tested negative (confirmed by at least two additional negative RT-PCR tests and clinical observation). The proposed AI system achieved an AUC of 0.92 and performed equally well in sensitivity compared to a senior thoracic radiologist on a testing set of 279 cases. The AI system also improved the detection of RT-PCR positive SARS-CoV-2 patients who presented with normal CTs, correctly identifying 17/25 (68%) patients, whereas all 25 RT-PCR SARS-CoV-2-positive CT-normal patients were classified as SARS-CoV-2 negative by radiologists.

Main Manuscript

The coronavirus disease 2019 (COVID-19) outbreak that originated in Wuhan, China^{1,2} has rapidly propagated due to widespread person-to-person transmission and has resulted in 1,113,758 cases in 197 countries and territories with a total of over 62,784 deaths as of April 5, 2020³⁻⁷. Early recognition of the disease is crucial not only for individual patient care related to rapid implementation of treatment, but also from a larger public health perspective to ensure adequate patient isolation and disease containment. Laboratory confirmation of SARS-CoV-2 is performed with a virus-specific reverse transcriptase polymerase chain reaction (RT-PCR), but the test can take up to two days to complete, and due to the possibility of false negatives serial testing may be required to reliably exclude infection. Chest computed tomography (CT) is a valuable component of evaluation and diagnosis in symptomatic patients with suspected SARS-CoV-2 infection. Chest CT is more sensitive and specific than chest radiography in evaluation of SARS-CoV-2 pneumonia, and there have been cases where CT findings were present prior to clinical symptomatology onset⁴. Nevertheless, chest CT findings are normal in some patients early in the disease course and therefore chest CT alone has limited negative predictive value to fully exclude infection⁸, highlighting the need to incorporate clinical information in the diagnosis. In the current climate of stress on healthcare resources due to the COVID-19 outbreak, including a shortage of RT-PCR test kits, there is an unmet need for rapid, accurate, unsupervised diagnostic tests for SARS-CoV-2. We propose that artificial intelligence (AI) algorithms may meet this need by integrating chest CT findings with clinical symptoms, exposure history, and/or laboratory testing in the algorithm. In our study, our proposed joint AI algorithm combining CT images and clinical history achieved an AUC of 0.92 when applied to a testing set of 279 cases. The AI model performed equally well in sensitivity as compared to a senior chest radiologist (AUC of 0.84), and out-performed a less experienced chest fellow (AUC of 0.73). When the AI model used only CT images or only clinical information the performance was lower (AUC of 0.86, and 0.80, respectively). The AI model with clinical information only and the joint AI model also improved the detection of SARS-CoV-2 RT-PCR-positive patients who presented with a normal CT, achieving a detection rate of 64% and 68% respectively, compared to radiologists who rated all such patients as SARS-CoV-2 (-). While the vast majority of suspected patients currently have little option but to wait for RT-PCR test results,

we propose that a highly robust AI algorithm has an important role for the rapid identification of SARS-CoV-2 patients which could be helpful in combating the current disease outbreak.

In December, 2019 the coronavirus disease 2019 (COVID-19) outbreak began in Wuhan, the capital city of central China's Hubei province. Initial reports show that the virus likely has a zoonotic origin related to the Huanan Seafood Market in Wuhan³⁻⁷. Approximately 16% of cases are severe⁹, and mortality is currently reported at 5.6% in China and 15.2% outside China as of March 1, 2020¹⁰. The World Health Organization (WHO) declared a global health emergency on January 30, 2020¹¹ and subsequently many countries have restricted travel to China to reduce the spread of disease. As of February 3, 2020, the death toll in China from SARS-CoV-2 surpassed SARS and MERS, which caused 349 and 848 deaths, respectively^{12,13}. Due to the alarming level of spread and severity, SARS-CoV-2 was characterized as a pandemic by WHO on March 11, 2020, the first pandemic caused by the new coronavirus¹⁴.

Chest computed tomography (CT) is a valuable tool for the early diagnosis and triage of patients suspected of SARS-CoV-2 infection. In an effort to control the spread of infection, physicians, epidemiologists, virologists, phylogeneticists, and others are working with public health officials and policymakers to better understand the disease pathogenesis. Early investigations have observed common imaging patterns on chest CT^{15,16}. For example, an initial prospective analysis in Wuhan revealed bilateral lung opacities on 40 of 41 (98%) chest CTs in infected patients and described lobular and subsegmental areas of consolidation as the most typical imaging findings⁴. Our initial study with chest CTs in 21 real-time RT-PCR assay confirmed patients also found high rates of ground-glass opacities and consolidation, sometimes with a rounded morphology and peripheral lung distribution⁸. A recent study has also shown that CT may demonstrate lung abnormalities in the setting of a negative RT-PCR test¹⁷. All this highlights the necessity for fast and accurate reporting of chest CTs.

During an outbreak of a highly infectious disease with person-to-person transmission, hospitals and physicians may have increased workloads and limited capabilities to triage and hospitalize suspected patients. Previous work demonstrated that early stage coronavirus patients may have negative findings on CT⁸, limiting radiologists' ability to reliably exclude disease. While waiting

6-48 hours for the confirmation of the SARS-CoV-2 coronavirus by RT-PCR, patients who are infected may spread the virus to other patients or caregivers if resources are not available to isolate patients who are only suspected to be infected; nosocomial infection was inferred in approximately 40% of cases in a recent large series¹⁸. Rapid detection of SARS-CoV-2 is imperative because an initial false negative could both delay treatment and increase risk of viral transmission to others. In addition, radiologists with expertise in thoracic imaging may not be available at every institution, increasing the need for AI aided detection.

Artificial intelligence (AI) may provide a method to augment early detection of SARS-CoV-2 infection. Our goal was to design an AI model that can identify SARS-CoV-2 infection based on the initial chest CT scans and associated clinical information that could rapidly identify SARS-CoV-2 (+) patients in the early stage. We collected chest CT scans and corresponding clinical information obtained at patient presentation. Clinical information included travel and exposure history, leukocyte counts (including absolute neutrophil number, neutrophil percentage, absolute lymphocyte number, and lymphocyte percentage), symptomatology (presence of fever, cough, and sputum), patient age, and patient sex.

We first developed a deep convolutional neural network (CNN) to learn the imaging characteristics of SARS-CoV-2 on the initial CT scan. We then used support vector machine (SVM), random forest, and multi-layer perceptron (MLP) classifiers to classify the SARS-CoV-2 patients according to the clinical information. MLP showed the best performance on the tuning set; only MLP performance is reported hereafter. Finally, we created a neural network model combining the radiologic data and the clinical information to predict SARS-CoV-2 status (Fig. 1).

A dataset of the presenting chest CT scans from 905 patients for whom there was a clinical concern of SARS-CoV-2 was acquired between Jan 17, 2020 and March 3, 2020 from 18 medical centers in 13 provinces in China. The data set included patients aged from 1 year to 91 years (40.7 year \pm 16.5 years), and included 488 men and 417 women. All subjects were acquired using a standard chest CT protocol and were reconstructed using the lung kernel and displayed with a lung window. A total of 419 patients (46.2%) tested positive for SARS-CoV-2 by laboratory-confirmed real-time RT-PCR assay and next-generation sequencing, while 486 patients (53.8%) tested negative

(confirmed by at least two additional negative RT-PCR tests and clinical observation). We randomly split the dataset into 60% training set (534 cases; 242 SARS-CoV-2 (+); 292 SARS-CoV-2 (-) cases), 10% tuning set (92 cases; 43 SARS-CoV-2 (+) cases; 49 SARS-CoV-2 (-) cases), 30% testing set (279 cases; 134 SARS-CoV-2 (+) cases; 145 SARS-CoV-2 (-) cases) (Extended Fig. 1).

We evaluated the AI models on the testing set and compared their performance to one fellowship trained thoracic radiologist with ten years of experience (A. J.) and one thoracic radiology fellow (S. S.). The same initial chest CT and clinical information were available to the radiologists as was provided to the AI model. Sensitivity, specificity and AUC were calculated for both human readers and the AI models. The performance of the AI model and human readers are demonstrated in Fig. 2 and Extended Fig. 2. The receiver operating characteristic (ROC) curve of the AI model is shown in Fig. 2.

The joint model using both clinical data and CT imaging achieved an 84.3% sensitivity (95% confidence interval (CI) 77.1%, 90.0%), an 82.8% specificity (95% CI 75.6%, 88.5%) and 0.92 AUC (95% CI 0.887, 0.948). The CNN mode that uses only CT imaging data had an 83.6% sensitivity (95% CI 76.2%, 89.4%; $p=1$), a 75.9% specificity (95% CI 68.1%, 82.6%; $p<0.05$) and 0.86 AUC (95% CI 0.821, 0.907; $p<0.01$). The multi-layer perceptron (MLP) model that uses only clinical data had an 80.6% sensitivity (95% CI 72.9%, 86.9%; $p=0.442$) and a 68.3% specificity (95% CI 60.0%, 75.8%; $p<0.001$) and 0.80 AUC (95% CI 0.746, 0.849; $p<0.001$). The senior thoracic radiologist using both the CT and clinical data achieved a 74.6% sensitivity (95% CI 66.4%, 81.7%; $p=0.05$), 93.8% specificity (95% CI 88.5%, 97.1%; $p<0.01$) and 0.84 AUC (95% CI 0.800, 0.884). The thoracic radiology fellow using both the CT and clinical data achieved a 56.0% sensitivity (95% CI 47.1%, 64.5%; $p<0.001$), 90.3% specificity (95% CI 84.3%, 94.6%, $p=0.09$) and 0.73 AUC (95% CI 0.683, 0.780). P-value indicates the significance of difference in performance metric compared with respect to the joint model.

With a higher AUC, the joint model integrating CT images and associated clinical information outperformed the model trained on CT images only and the clinical model trained on clinical information only. The joint model, the CT model and the clinical model performed equally well in

sensitivity compared to the senior thoracic radiologist but showed statistically significant improvement in sensitivity compared to the thoracic fellow (Fig. 2).

The testing set contained 25 SARS-CoV-2 (+) patients with a chest CT identified as normal by both of the reading radiologists at presentation. The CNN model identified 13/25 (52%) scans as SARS-CoV-2 (+), the clinical model classified 16/25 (64%) as disease positive, and the joint model classified 17/25 (68%) as disease positive, whereas the senior chest radiologist and the chest radiology fellow identified 0/25 (0%) of these scans as disease positive.

We summarized the comparisons of prediction between the joint model and the radiologists in the Extended Fig. 4. Of the 134 SARS-CoV-2 (+) cases in the testing set, 90 out of 134 cases were correctly classified by both the joint model and the senior thoracic radiologist. Forty-four out of 134 cases were classified differently by the joint model and the senior thoracic radiologist. Of the 44 cases, 33 cases were correctly classified positive by the joint model, but were misclassified by the senior thoracic radiologist. Ten cases were classified negative by the joint model, but correctly diagnosed by the senior thoracic radiologist. No cases were misclassified by both the joint model and the senior thoracic radiologist.

Of the 145 SARS-CoV-2 (-) cases in the testing set, 113 out of 145 cases were correctly classified by both the joint model and the senior thoracic radiologist. Thirty-two out of 145 cases were classified differently by the joint model and the senior thoracic radiologist. Seven cases were correctly classified negative by the joint model, but were diagnosed positive by the senior thoracic radiologist. Twenty-three cases were classified positive by the joint model, but correctly diagnosed negative by the senior thoracic radiologist. Two cases were misclassified by both the joint model and the senior thoracic radiologist.

Chest CT is a well-known diagnostic tool for evaluation of patients with a suspected pulmonary infection. During the outbreak of SARS-CoV-2 in some countries including China and South Korea, chest CT has been widely used in clinical practice due to its speed and availability. Most institutions in China have adopted a policy of performing a chest CT scan on any patient with fever and a suspicion of SARS-CoV-2 infection. Initial experience with CT has demonstrated that

typical findings are multilobular and bilateral and include both ground glass opacities and consolidation, often with a peripheral lung distribution. Pleural effusions, lymphadenopathy, and discrete pulmonary nodules are very uncommon^{8,19,20}.

According to the recommendations of the WHO, the most accurate diagnosis of SARS-CoV-2 is nucleic acid detection²¹ in secretional fluid collected from a throat swab using RT-PCR. However, there is a shortage of the nucleic acid detection kits and results can take up to two days. Chest CT has also been proposed as an important diagnostic tool. A chest CT study can be obtained and interpreted much more quickly than RT-PCR. While chest CT is not as accurate as RT-PCR in detecting the virus it may be a useful tool for triage in the period before definitive results are obtained^{9,22}. For patients with mild symptoms demonstrating normal chest CT in the early stage, our model showed that clinical information played a role in the accurate diagnosis of SARS-CoV-2.

There are two potential limitations to the use of chest CT. First, the health system during an epidemic may be overburdened, which may limit timely interpretation of the CT by a radiologist. Second, the morphology and severity of pathologic findings on CT is variable. In particular, mild cases may have few if any abnormal findings on chest CT.

We believe implementation of the joint algorithm discussed above could aid in both issues. First, the AI algorithm could evaluate the CT immediately after completion. Secondly, the algorithm outperformed radiologists in identifying SARS-CoV-2 (+) patients demonstrating normal CT results in the early stage. Thirdly, the algorithm performed equally well in sensitivity ($p=0.05$) in the diagnosis of SARS-CoV-2 as compared to a senior thoracic radiologist. Specifically, the joint algorithm achieved a statistically significant 6% ($p<0.01$) and 12% ($p<0.001$) improvement in AUC as compared to the CNN model using only CT images and the MLP model using only clinical information respectively. The AI model could be deployed as an application that can run on a simple workstation alongside the radiologists. Use of the AI tool would require integration with the Radiology PACS and clinical database systems or other image storage database, which is relatively easy to achieve in modern hospital systems. The AI system could be implemented as a rapid diagnostic tool to flag suspected SARS-CoV-2 patients when CT images and/or clinical

information are available, and radiologists could review these suspected cases identified by AI with a higher priority.

Our proposed model does have some limitations. One major limitation of this study is the limited sample size. Despite the promising results of using the AI model to screen SARS-CoV-2, further data collection is required to test the generalizability of the AI model to other patient populations. Collaborative effort in data collection may facilitate improving the AI model. Difficulties on model training also arise due to the limited sample size. In this work we used a pre-trained TB model to select key slices to represent a full 3D CT scan. This approach can reduce computation of training a 3D convolution neural network, with a trade off on missing information in the slices that are not selected for model training and inference. The design of the CNN model offers a natural visualization to explain the prediction. We showcased some examples allowing the AI models to be cross referenced with radiologist's findings (Fig. 3). However, there are examples in which the visualization fails to provide a clear explanation. We do not know if the model incorporates features such as airways, background of emphysema or the border of the lung in its prediction. Another limitation is the bias towards SARS-CoV-2 patients in the training data, which, given the non-specific nature of the ground glass opacity and other features on chest CT images, potentially limits the usefulness of the current AI model to distinguish SARS-CoV-2 from other causes of respiratory failure. Therefore, our algorithm may be helpful in places with current high rates of COVID-19 disease, but is unlikely to provide as much usefulness in places or times where SARS-CoV-2 prevalence is low.

In future studies, a larger dataset will be collected as the scale of this outbreak is climbing. We aim to explore different approaches in convolutional neural networks including three-dimensional deep learning models and improvement of interpretability of CNN models. The generalizability of the AI system evaluated at multiple centers will be necessary to validate the robustness of the models.

In conclusion, these results illustrate the potential role for a highly accurate AI algorithm for the rapid identification of SARS-CoV-2 patients which could be helpful in combating the current disease outbreak. We believe the AI model proposed, that combines CT imaging and clinical information, and shows equivalent accuracy to a senior chest radiologist, could be a useful

screening tool to quickly diagnose infectious diseases such as SARS-CoV-2 that does not require radiologist-input or physical tests.

Methods

Study participants

The study was approved by the institutional review board of each participating hospital in China and the Icahn School of Medicine at Mount Sinai in New York. The institutional review boards waived the requirement to obtain written informed consent for this retrospective study, which evaluated de-identified data and involved no potential risk to patients. To avert any potential breach of confidentiality, no link between the patients and the researchers was made available.

We collected the initial chest CT studies and clinical data from 905 patients presenting between January 17 and March 3, 2020 to one of 18 centers in 13 provinces in China where patients had SARS-CoV-2 exposure, fever and a RT-PCR test for SARS-CoV-2. The exposure of SARS-CoV-2 is defined as either 1) travel history to Wuhan for patients collected outside of Wuhan, or travel to the animal market within 30 days of the symptom onset for patients who live in Wuhan or 2) close contact with patients with RT-PCR confirmed SARS-CoV-2 infection for all patients. Of the 905 patients included in the study, 419 had a positive RT-PCR test while 486 had a negative test (confirmed by at least two additional negative RT-PCR tests and clinical observation).

Clinical Information

Patient's age, sex, exposure history, symptoms (present or absent of fever, cough and/or sputum), white blood cell counts, absolute neutrophil number, neutrophil percentage, absolute lymphocyte number and lymphocyte percentage were collected (Table 1). Sex, exposure history and symptoms were categorical variables. We used the LabelEncoder function in scikit-learn package to encode the target categorical variables into numerical variables with value between 0 and 1. Then, we normalized each feature within a range of 0 and 1 using MinMaxScaler function in the scikit-learn package for further model development.

Reader studies

The predictions of the AI models were compared to two radiologists on the testing set. Both radiologists were board-certified (A.J. chest fellowship trained with 10 years' clinical experience; S.S. a current chest radiology fellow). The readers were given patients' initial CT scan (at presentation) and associated clinical history that were used to test the AI models. Each reader independently reviewed the same set and evaluated the initial CT scan and clinical details, and combined imaging and clinical data in their review in a manner consistent with their clinical practice. Using this data, they predicted the SARS-CoV-2 status of the patients. Their predictions were compared to those of the AI algorithm and the RT-PCR results.

AI Models

The RT-PCR virology test (SARS-CoV-2 (+) or SARS-CoV-2 (-)) was used as the reference to train the models. We developed and evaluated three different models using CT images and clinical information. Firstly, a deep learning model using a convolutional neural network (Model 1) was developed to only use CT images to predict SARS-CoV-2 status. Secondly, conventional machine learning methods (Model 2), including support vector machine (SVM), random forest and multi-layer perceptron (MLP), were evaluated to predict SARS-CoV-2 using only clinical information. Finally, we created a joint convolutional neural network model (Model 3) combining the radiologic data and the clinical data.

Convolutional Neural Network Model (Model 1)

We proposed a CNN-based AI system to diagnose SARS-CoV-2 using a full CT scan of the chest. Similar to the previously reported AI diagnosis system^{23,24}, our algorithm consisted of two CNN subsystems to firstly identify the abnormal CT slices and then to perform region-specific disease diagnosis (Fig. 1). More specifically, the slice selection CNN was trained to evaluate a chest CT slice and assign a probability that it was normal. The inverse of this probability was then used to rank the abnormal slices of each CT scan. We selected the 10 most abnormal slices from each study for the subsequent disease diagnosis due to the tradeoff of efficiency and turn-around time. The disease diagnosis CNN was designed to classify SARS-CoV-2 patients using multiple instance learning. The CNN was trained to predict whether a CT slice is from a SARS-CoV-2 (+) or SARS-

CoV-2 (-) patient. The average probability from the 10 abnormal CT slices from each patient's study was used to generate a prediction of SARS-CoV-2 status for the patient.

Image Preprocessing

The first step is to select pertinent slices from the hundreds of images produced by a CT scan. Pertinent images contain pulmonary tissue and a potential parenchymal abnormality. For the selection of pertinent slices, image segmentation was used to detect parenchymal tissue. The raw CT images all had a 512 x 512 matrix storing CT intensities in Hounsfield Units (HU). A standard lung window (width (w)=1500 HU and level (l)=-600 HU) was used to normalize each slice to pixel intensities between 0 and 255. We segmented CT images into two parts, body and lung. The body part was segmented by finding the largest connected component consisting of pixels with an intensity greater than 175. The segmented connected component was filled into a solid region. The lung region was defined as the pixels with intensity less than 175 that fall within the segmented body part. Small regions with less than 64 pixels were removed, as they are typically segmented due to random noise. The lung region was enlarged by 10 pixels to fully include the pleural boundary. We discard images if the size of the lung was smaller than 20% of the size of the body part.

1) Slice Selection CNN

We used Inception-ResNet-v2²⁵ as the slice selection CNN to identify abnormal CT images from all chest CT images²⁶. The slice selection CNN was pre-trained in a previous TB detection study on CT images from a total of 484 non-TB pneumonia patients, including bacterial pneumonia, viral pneumonia and fungal pneumonia, in addition to 439 pulmonary tuberculosis (PTB) and 155 normal chest CT patients. For CT images, the TB model predicts the probabilities of 3 classes, including pulmonary tuberculosis (PTB), non-TB pneumonia and normal chest CT. This model achieved 99.4% accuracy in differentiating normal slices from abnormal (PTB and non-TB pneumonia) slices. In this work, we applied the TB model to a full CT scan to select 10 slices with the lowest probability of being normal. We noted that these selected slices may show no abnormal findings if the SARS-CoV-2 (+/-) patient's CT is normal.

2) Disease Diagnosis CNN

We used the 18-layer residual network (ResNet-18²⁷) as the disease diagnosis CNN. The ResNet-18 takes images of segmented lungs as input and outputs probability of SARS-CoV-2 positivity. A max pooling layer that outputs log probability was used at the last layer, instead of the standard design that uses an average pooling layer at the last layer. The rationale of this design is that, given the abnormal finding is usually localized in a subregion of a CT image, we would like to predict whether a small region is abnormal due to SARS-CoV-2²⁸. The CNN model can then be seen as a classifier that reports whether its receptive field is SARS-CoV-2 (+). The label of an image is then predicted by combining all predictions of every local region over the whole image. Max pooling serves as an “OR” gate that labels an image as SARS-CoV-2 (+) if there is any subregion in it that is SARS-CoV-2 (+). Patient level prediction was set as the average of image-level prediction of a patient’s 10 most abnormal images. To visualize the CNN’s prediction, we up-sampled the CNN’s outputs, without applying the max pooling layer, to the original image size. The lung mask was applied to up-sampled outputs for clear visualization.

3) CNN Training

We used binary cross entropy as the objective function. Adam optimizer²⁹ with a learning rate 0.001 was used to train the neural network. The learning rate was decreased by a factor of 0.95 each epoch. We applied random rotation, grid distortion, and cutout³⁰ to images for data augmentation. 20% of training samples were held out as the tuning set to monitor the progress of the training process. The training process was iterated for 40 epochs with a batch size of 16 samples. Performance on the tuning set was monitored every 100 iterations. The model with lowest binary cross entropy on the tuning set was selected as the final model. Parameters were tuned to ensure that the validation error decreases along with the training error.

We designed a weakly supervised task to initialize weights of the CNN model. Specifically, we randomly selected image patches of lung regions from training images and labeled those patches as the label of the training images. The CNN is then pre-trained to classify these image patches for 1 epoch. This weakly supervised task accords with the idea that the CNN is classifying a local region in the CT image to be SARS-CoV-2 (+/-).

Machine Learning Classifiers (Model 2)

We developed support vector machine, random forest and multi-layer perceptron classifiers based on patients' age, sex, exposure history, symptoms (present or absent of fever, cough and/or sputum), white blood cell counts, neutrophil counts, neutrophil percentage, lymphocyte counts and lymphocyte percentage. We fine-tuned the hyperparameters of each classifier on the training set and tuning set, and evaluated the best model on the testing set. For the support vector machine classifier, we assessed the "C", and kernel. For the random forest classifier, the number of estimators was tuned. For multi-layer perceptron, we assessed the number of layers and the number of hidden nodes in each layer. After the hyperparameter optimization, a 3-layer MLP model with 64 nodes in each layer was selected because of the highest AUC score on the tuning set. The MLP model was selected because of the highest AUC score on the tuning set (Extended Fig. 3). We used the Scikit-learn³² package to fit and evaluate these models.

Joint Model: Combining CT imaging and clinical information (Model 3)

We trained a model to integrate CT imaging data and clinical information. We applied the global averaging layer to the last layers of the convolutional model described previously to derive a 512 dimensional feature vector to represent a CT image. A total of 12 clinical features (Table 1) of the same patient were concatenated with this feature vector. A MLP takes this combined feature vector as the input to predict the status of SARS-CoV-2. We used a 3-layer MLP, each layer has 64 nodes and is composed by a batch normalization layer, a fully connected layer and a ReLU activation function. Normalized Gaussian noise was added at the input layers for data augmentation. The MLP was jointly trained with the CNN. We applied binary cross entropy to validate the predictions from both MLP and CNN during the training process. The sum of these two measurements was used as the overall objective function to train the joint model. We used the same optimization strategy of Model 1 to train the MLP and CNN, except that the learning rate was increased to 0.002. The CNN was also initialized by the weakly supervised task of classifying the small image patches.

Statistical analysis

The two-sided 95% confidence interval of sensitivity and specificity was calculated by the exact method³³. The confidence interval of AUC was calculated by the DeLong methods³⁴. McNemar's test³⁵ was used to compare the performance between models and human readers. The Youden index was used to determine the optimal model sensitivity and specificity. Statistical significance was defined as a p-value less than 0.05. Logistic regression was used to evaluate the significance of each clinical variable. Hosmer-Lemeshow goodness of fit³⁶ was used to assess the goodness of fit of the logistic regression. The statistics of AUC comparisons were computed in the *pROC* package³⁷. Other statistics were computed in python 3.6.5.

Data Availability

The datasets used in this study are not publicly available due to ethical considerations.

Code Availability

The code used for training the models is available at https://github.com/howchihlee/COVID19_CT. Implementations of our work is based on following open source repositories: Tensorflow: <https://www.tensorflow.org>; Pytorch: <https://pytorch.org> ; Keras: <https://keras.io>; Sklearn: <https://scikit-learn.org/stable/>;

Figures and Tables

Table 1. Characteristics of Patient’s Clinical Information. The p-value of each clinical feature was tested by logistic regression. The Hosmer-Lemeshow goodness of fit was used to assess the logistic regression fit. Patient’s age, presence of exposure to SARS-CoV-2, presence of fever, cough and cough with sputum and white blood cell counts were significant features associated with SARS-CoV-2 status. The logistic regression was a good fit ($p=0.66$).

	COVID-19 positive (n=419)	COVID-19 negative (n=486)	p-value
Sex			
Men	208 (49.6)	280 (57.6)	0.36
†Age (years)	43.0±16.4 (32, 54)	38.6±16.3 (27, 48)	<0.001
Temperature (°C)	37.6±0.9	37.5±1.0	0.60
Exposure history	319 (76.1)	254 (52.3)	<0.001
Clinical symptoms			
Fever	314 (75.0)	318 (65.4)	<0.01
Cough	210 (50.1)	128 (26.3)	<0.001
Cough with sputum	83 (20.0)	177 (36.4)	<0.001
Laboratory findings			
†WBC (10 ⁹ /L)	5.4±2.2 (4.0, 6.4)	8.3±3.4 (6.1, 10.0)	<0.05
†Neutrophils (10 ⁹ /L)	3.5±1.9 (2.3, 4.2)	5.9±3.1 (3.7, 7.4)	0.11
†Neutrophils Percentage	63.0±14.7 (53.8, 74.2)	68.9±13.1 (60.7, 78.8)	0.30
†Lymphocytes (10 ⁹ /L)	1.4±0.8 (0.9, 1.7)	1.6±0.9 (1.0, 2.0)	0.12
†Lymphocytes Percentage	26.4±12.5 (17.3, 34.5)	21.3±11.1 (12.7, 28.9)	0.53

† Data in parenthesis shows Interquartile Range (IQR)

Other data in parenthesis shows percentage

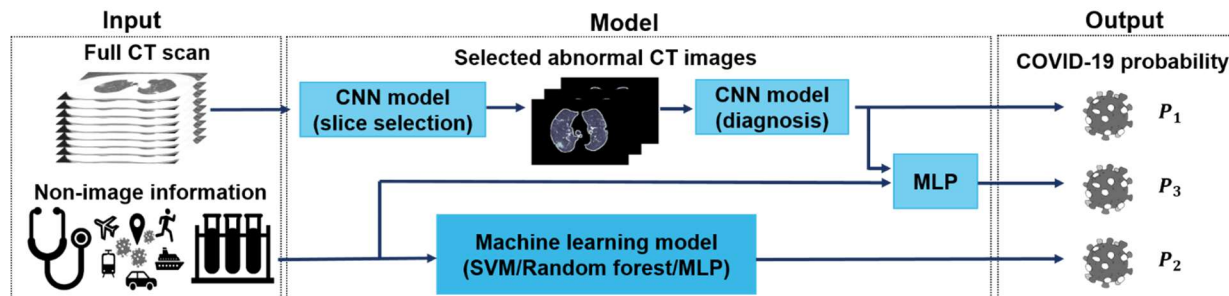


Fig. 1. Illustration of the modelling framework. The three AI models generate the probability of a patient being SARS-CoV-2 (+); the first based on a chest CT scan; the second based on clinical information; and the third, an aggregation of the chest CT and clinical information. For evaluation of the chest CT, every slice was first ranked by the probability of finding a parenchymal abnormality, as predicted by the convolutional neural network model (slice selection CNN) which was a pre-trained TB model. The top 10 abnormal CT images were put in to the second CNN (diagnosis CNN) to predict the likelihood of SARS-CoV-2 positivity (P_1). Demographic and clinical data (patient's age and sex, exposure history, symptoms and laboratory tests) were put into a machine learning model to classify SARS-CoV-2 positivity (P_2). Features generated by the diagnosis CNN model and the non-imaging clinical information machine learning model were integrated by a multi-layer perceptron network (MLP) to make the final output of the joint model (P_3).

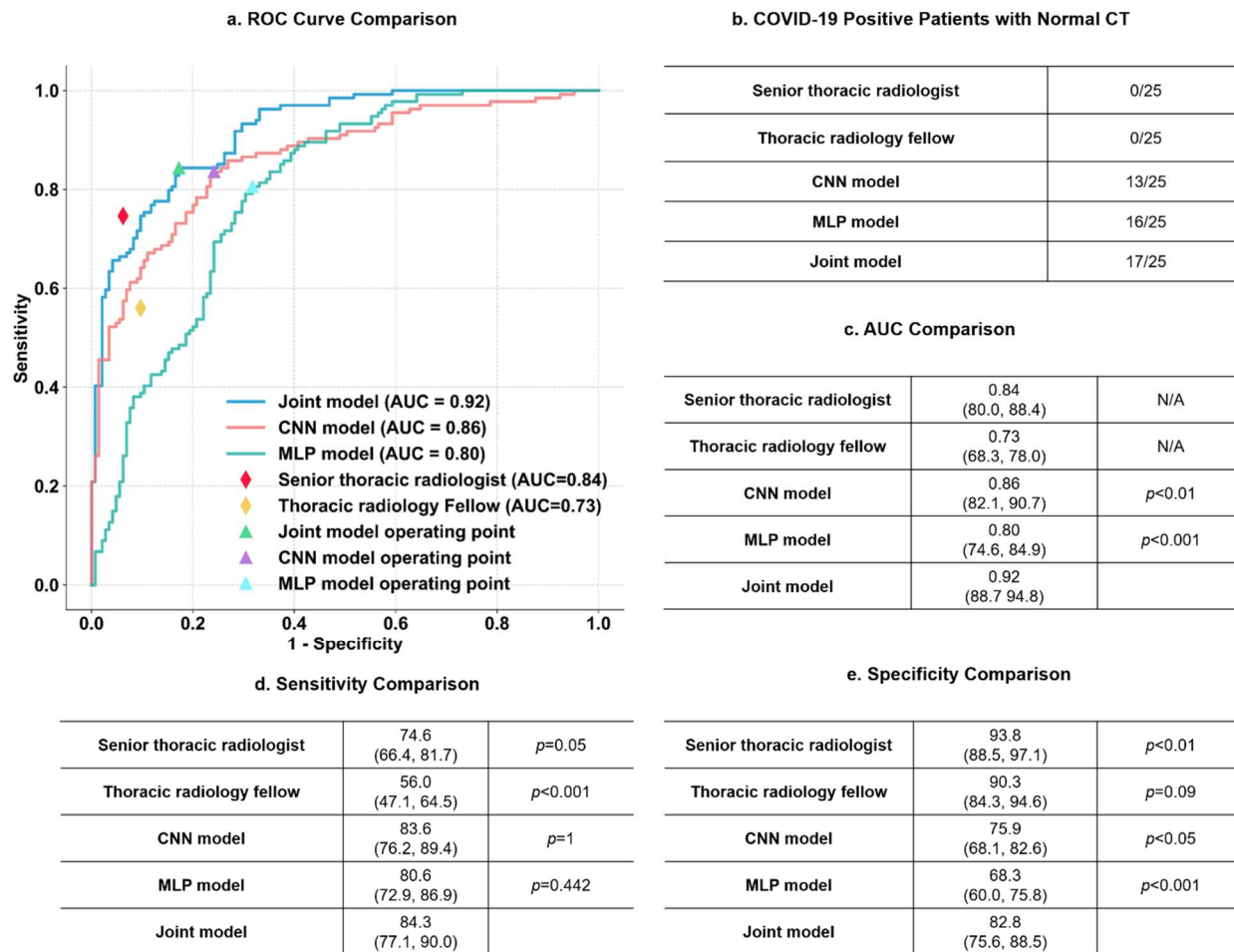


Fig. 2. Results of the AI models on the testing set. The statistical tests were calculated by comparing the joint model to the CNN model, the MLP model and the two human readers. The AUC comparisons were evaluated by the DeLong test. Sensitivity and specificity comparisons were calculated by using the exact method to compute the 95% confidence interval shown in parenthesis and the McNemar's test to calculate the p-value. a, ROC Curve comparison of the joint model, the CNN model trained based on CT images, the MLP model trained based on clinical information and two readers. b, Comparison of the success rate of diagnosing SARS-CoV-2 positive patients with normal CT scans. The joint model integrating CT imaging and clinical information identified 17/25 (68%) patients, the CNN model identified 13/25 (52%) and the MLP model identified 16/25 (64%) while radiologists, also using both CT imaging and clinical information, correctly diagnosed 0/25 CT scans. c, AUC comparison between the proposed models and human readers. The joint model achieved an area under the curve score of 0.92. The CNN

model achieved an AUC score of 0.86. The MLP model achieved an AUC score of 0.80. The senior thoracic radiologist achieved an AUC score of 0.84. The thoracic radiology fellow achieved an AUC score of 0.73. d, Sensitivity comparisons between the AI model and human readers. e, Specificity comparisons between the AI model and human readers.

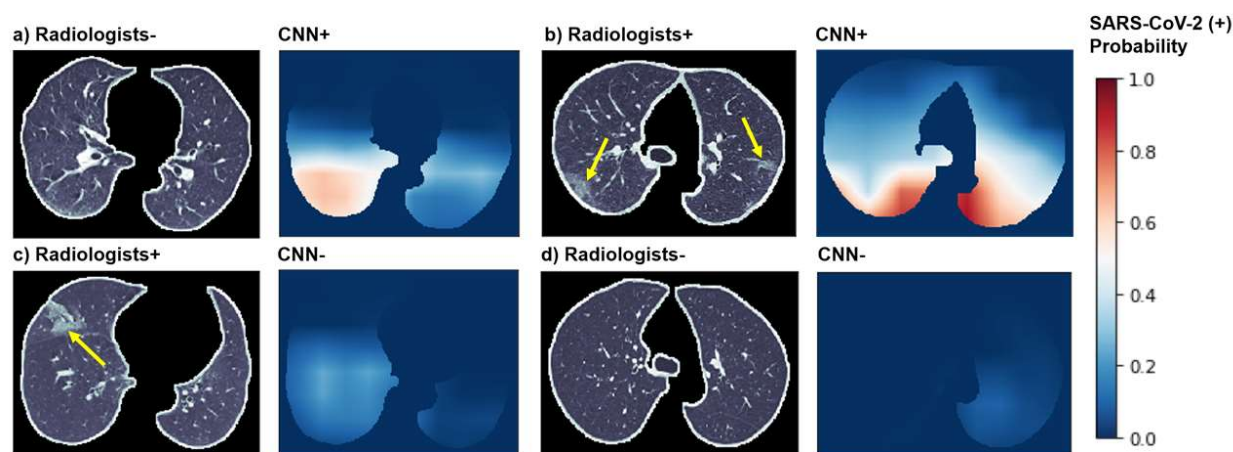


Fig. 3. Examples of CT images of SARS-CoV-2 (+) patients and visualization of features correlated to SARS-CoV-2 presented predictions by the CNN model as a fair comparison to radiologists. For each set, the left image has the segmented lung used as input for the CNN model. The right image demonstrates the heatmap of pixels (red color indicates higher probability) that the CNN model classified as having SARS-CoV-2 affected lung. (a) A 51-year-old female with fever and history of exposure to SARS-CoV-2. The CNN model identified abnormal features in the right lower lobe (white color), while two radiologists labeled this CT as negative. (b) A 52-year-old female who had history of exposure to SARS-CoV-2 and presented with fever and productive cough. Segmented CT image of the lung shows peripheral ground-glass opacities (arrows) in the bilateral lungs that radiologists labeled, with corresponding CNN model predicting SARS-CoV-2 involvement in matching areas. (c) A 72-year-old female with exposure history to the animal market in Wuhan and presented with fever and productive cough. Segmented CT image shows ground-glass opacity in the anterior aspect of the right lung (arrow), with corresponding CNN model predicting absence of disease. (d) A 59-year-old female with cough and exposure history. Segmented CT shows no evidence of pneumonia, with corresponding CNN model also predicting absence of disease.

	Training Set (n=534)	Tuning Set (n=92)	Testing Set (n=279)
Sex			
Men	278 (52.1)	51 (55.4)	159 (57.0)
†Age (years)	40.6±16.3 (29, 51)	36.5±13.9 (26, 45)	42.1±17.5 (30, 55)
Temperature (°C)	37.5±1.0	37.5±0.9	37.6±0.9
Exposure history	330 (61.8)	53 (63.9)	190 (68.3)
Clinical symptoms			
Fever	371 (69.5)	59 (64.1)	202 (72.4)
Cough	185 (34.6)	34 (37.0)	119 (42.7)
Cough with sputum	165 (30.9))	26 (28.3)	69 (24.7)
Laboratory findings			
†WBC (10 ⁹ /L)	7.1±3.4 (4.7, 8.7)	6.8±2.5 (5.2, 7.9)	6.8±3.2 (4.7, 8.4)
†Neutrophils (10 ⁹ /L)	5.0±3.0 (2.9, 6.2)	4.7±2.3 (3.2, 5.3)	4.5±2.8 (2.6, 5.7)
†Neutrophils Percentage	67.2±13.9 (58.1, 78.0)	66.9±12.7 (60.4, 75.7)	63.7±15.0 (55.0, 74.5)
†Lymphocytes (10 ⁹ /L)	1.5±0.8 (0.9, 1.9)	1.5±0.6 (1.0, 1.8)	1.6±1.1 (1.0, 1.9)
†Lymphocytes Percentage	22.9±11.9 (13.9, 31.2)	22.9±9.5 (16.5, 30.1)	25.4±12.7 (16.0, 32.7)

Extended Fig. 1. Characteristics of clinical features in the training set, tuning set and testing set.

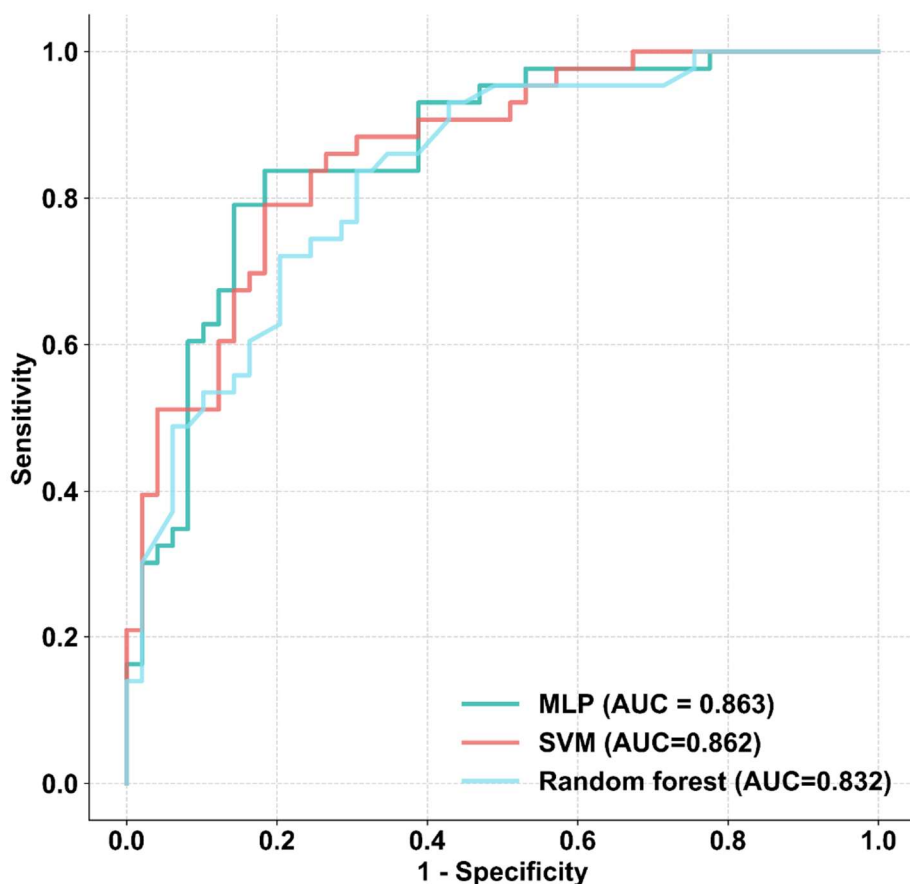
† Data in parenthesis shows Interquartile Range (IQR)

Other data in parenthesis shows percentage

Diagnostic Performance Comparison Between AI Models and Human Readers

	Accuracy	Positive Predictive Value	Negative Predictive Value
Senior thoracic radiologist	84.6 (79.8, 88.6)	91.7 (85.4, 95.5)	80.0 (74.9, 84.3)
Thoracic radiology fellow	73.8 (68.3, 78.9)	84.3 (76.1, 90.0)	69.0 (64.6, 73.0)
CNN model	79.6 (74.4, 84.1)	76.2 (70.4, 81.2)	83.3 (77.2, 88.1)
MLP model	74.2 (68.6, 79.2)	70.1 (64.6, 75.1)	79.2 (72.6, 84.6)
Joint model	83.5 (78.6, 87.7)	81.9 (75.9, 86.7)	85.1 (79.3, 89.5)

Extended Fig. 2. Comparisons of the diagnostic performance between AI models and human readers. Data were presented in percentage and the 95% confidence interval.



Extended Fig. 3. ROC curve comparison of the MLP, random forest and SVM models on the tuning set. P-value indicates the significance of difference in performance metric compared with respect to the MLP model by using the DeLong test. The MLP showed no significant difference as compared to the SVM model ($p=0.98$) and the random forest model ($p=0.35$). The MLP model was selected in this study due to the highest AUC score.

a. Comparison of predictions by the composite AI model and the senior thoracic radiologist

	SARS-CoV-2 (+) Patients (n=134)		SARS-CoV-2 (-) Patients (n=145)
Joint Model (+) Senior Thoracic Radiologist (+)	90	Joint Model (-) Senior Thoracic Radiologist (-)	113
Joint Model (+) Senior Thoracic Radiologist (-)	34	Joint Model (-) Senior Thoracic Radiologist (+)	7
Joint Model (-) Senior Thoracic Radiologist (+)	10	Joint Model (+) Senior Thoracic Radiologist (-)	23
Joint Model (-) Senior Thoracic Radiologist (-)	0	Joint Model (+) Senior Thoracic Radiologist (+)	2

b. Comparison of predictions by the composite AI model and the thoracic radiology fellow

	SARS-CoV-2 (+) Patients (n=134)		SARS-CoV-2 (-) Patients (n=145)
Joint Model (+) Thoracic Radiology Fellow (+)	68	Joint Model (-) Thoracic Radiology Fellow (-)	108
Joint Model (+) Thoracic Radiology Fellow (-)	44	Joint Model (-) Thoracic Radiology Fellow (+)	12
Joint Model (-) Thoracic Radiology Fellow (+)	7	Joint Model (+) Thoracic Radiology Fellow (-)	23
Joint Model (-) Thoracic Radiology Fellow (-)	15	Joint Model (+) Thoracic Radiology Fellow (+)	2

Extended Fig. 4. Comparisons of predictions by the joint model and human readers. The (+/-) indicates the prediction of the SARS-CoV-2 status by the joint model and human readers.

References

1. Zhu, N., *et al.* A novel coronavirus from patients with pneumonia in China, 2019. *N Engl J Med* (2020).
2. Tan, W., *et al.* A novel coronavirus genome identified in a cluster of pneumonia cases—Wuhan, China 2019–2020. *China CDC Weekly* 2020; 2 (4): 61-2.
3. Chan, J.F., *et al.* A familial cluster of pneumonia associated with the 2019 novel coronavirus indicating person-to-person transmission: a study of a family cluster. *The Lancet* **395**, 514-523 (2020).
4. Huang, C., *et al.* Clinical features of patients infected with 2019 novel coronavirus in Wuhan, China. *The Lancet* **395**, 497-506 (2020).
5. Phan, L.T., *et al.* Importation and Human-to-Human Transmission of a Novel Coronavirus in Vietnam. *N Engl J Med* **382**, 872-874 (2020).
6. Li, Q., *et al.* Early Transmission Dynamics in Wuhan, China, of Novel Coronavirus-Infected Pneumonia. *N Engl J Med* (2020).
7. World Health Organization. Coronavirus disease 2019 (SARS-COV-2): situation report, 76. (2020).
8. Chung, M., *et al.* CT Imaging Features of 2019 Novel Coronavirus (2019-nCoV). *Radiology* **295**, 202-207 (2020).
9. Guan, W.J., *et al.* Clinical Characteristics of Coronavirus Disease 2019 in China. *N Engl J Med* (2020).
10. Baud, D., *et al.* Real estimates of mortality following SARS-COV-2 infection. *Lancet Infect Dis* (2020).

11. Mahase, E. China coronavirus: WHO declares international emergency as death toll exceeds 200. *BMJ* **368**, m408 (2020).
12. Lam, C.W., Chan, M.H. & Wong, C.K. Severe acute respiratory syndrome: clinical and laboratory manifestations. *Clin Biochem Rev* **25**, 121-132 (2004).
13. Azhar, E.I., Hui, D.S.C., Memish, Z.A., Drosten, C. & Zumla, A. The Middle East Respiratory Syndrome (MERS). *Infect Dis Clin North Am* **33**, 891-905 (2019).
14. World Health Organization. WHO Director-General's opening remarks at the media briefing on SARS-CoV-2 (-) 11 March 2020. (2020, March 11).
15. Phelan, A.L., Katz, R. & Gostin, L.O. The Novel Coronavirus Originating in Wuhan, China: Challenges for Global Health Governance. *JAMA* (2020).
16. Nishiura, H., *et al.* The Extent of Transmission of Novel Coronavirus in Wuhan, China, 2020. *J Clin Med* **9**(2020).
17. Xie, X., *et al.* Chest CT for Typical 2019-nCoV Pneumonia: Relationship to Negative RT-PCR Testing. *Radiology*, 200343 (2020).
18. Wang, D., *et al.* Clinical Characteristics of 138 Hospitalized Patients With 2019 Novel Coronavirus-Infected Pneumonia in Wuhan, China. *JAMA* (2020).
19. Kanne, J.P. Chest CT Findings in 2019 Novel Coronavirus (2019-nCoV) Infections from Wuhan, China: Key Points for the Radiologist. *Radiology* **295**, 16-17 (2020).
20. Song, F., *et al.* Emerging 2019 Novel Coronavirus (2019-nCoV) Pneumonia. *Radiology* **295**, 210-217 (2020).

21. World Health Organization. Clinical management of severe acute respiratory infection when novel coronavirus (2019-nCoV) infection is suspected: interim guidance, 28 January 2020. (WHO, 2020).
22. Ai, T., *et al.* Correlation of Chest CT and RT-PCR Testing in Coronavirus Disease 2019 (SARS-COV-2) in China: A Report of 1014 Cases. *Radiology*, 200642 (2020).
23. Liu, F., *et al.* Deep Learning Approach for Evaluating Knee MR Images: Achieving High Diagnostic Performance for Cartilage Lesion Detection. *Radiology* **289**, 160-169 (2018).
24. Liu, F., *et al.* Fully Automated Diagnosis of Anterior Cruciate Ligament Tears on Knee MR Images by Using Deep Learning. *Radiol Artif Intell* **1**, 180091 (2019).
25. Szegedy, C., Ioffe, S., Vanhoucke, V. & Alemi, A.A. Inception-v4, inception-resnet and the impact of residual connections on learning. in *Thirty-first AAAI conference on artificial intelligence* (2017).
26. Wang, Y., *et al.* A Generalized Deep Learning Approach for Evaluating Secondary Pulmonary Tuberculosis on Chest Computed Tomography. *SSRN* (2019).
27. He, K., Zhang, X., Ren, S. & Sun, J. Deep residual learning for image recognition. in *Proceedings of the IEEE conference on computer vision and pattern recognition* 770-778 (2016).
28. Oquab, M., Bottou, L., Laptev, I. & Sivic, J. Is object localization for free?-weakly-supervised learning with convolutional neural networks. in *Proceedings of the IEEE conference on computer vision and pattern recognition* 685-694 (2015).
29. Kingma, D.P. & Ba, J. Adam: A method for stochastic optimization. *arXiv preprint arXiv:1412.6980* (2014).

30. DeVries, T. & Taylor, G.W. Improved regularization of convolutional neural networks with cutout. *arXiv preprint arXiv:1708.04552* (2017).
31. Russakovsky, O., *et al.* Imagenet large scale visual recognition challenge. *International journal of computer vision* **115**, 211-252 (2015).
32. Pedregosa, F., *et al.* Scikit-learn: Machine learning in Python. *Journal of machine learning research* **12**, 2825-2830 (2011).
33. Agresti, A. & Coull, B.A. Approximate is better than “exact” for interval estimation of binomial proportions. *The American Statistician* **52**, 119-126 (1998).
34. DeLong, E.R., DeLong, D.M. & Clarke-Pearson, D.L. Comparing the areas under two or more correlated receiver operating characteristic curves: a nonparametric approach. *Biometrics*, 837-845 (1988).
35. McNemar, Q. *Psychological statistics*, (Wiley New York, 1962).
36. Hosmer, D.W., Hosmer, T., Le Cessie, S. & Lemeshow, S. A comparison of goodness-of-fit tests for the logistic regression model. *Statistics in medicine* **16**, 965-980 (1997).
37. Robin, X., *et al.* pROC: an open-source package for R and S+ to analyze and compare ROC curves. *BMC bioinformatics* **12**, 77 (2011).